SOX21 suppresses GBM growth by repressing AP-1 regulated target genes.

Eltjona Rrapaj[1], Juan Yuan[1], Idha Kurtsdotter[1], Vsevolod Misyurin[1], Guido Baselli[2,3], Oscar Persson[4], Maria Bergsland[1] and Jonas Muhr[1,*]

[1]Department of Cell and Molecular Biology, Karolinska Institutet, SE-17177 Stockholm, Sweden.

[2]Department of Microbiology, Tumor and Cell Biology, Karolinska Institutet, SE-17177 Stockholm, Sweden.

[3]Science for Life Laboratory, C1 Pelechano, SE-17121, Solna, Sweden.

[4]Department of Neurosurgery, Karolinska University Hospital, and Department of Clinical Neuroscience, Karolinska Institutet, SE-17176 Stockholm, Sweden.

* Corresponding author: Jonas Muhr, e-mail: jonas.muhr@ki.se, phone: +46-70-6805017

Abstract

Resistance of glioblastoma stem cells (GSCs) to standard treatments is a major cause of glioblastoma (GBM) recurrence. This study examines the potential of the transcription factor SOX21 to inhibit GSC properties and combat GBM progression. Results show that increasing SOX21 levels in primary GSCs induces an anti-tumorigenic gene expression profile, which is substantiated by a significant correlation between high SOX21 expression and improved survival rates of GBM patients. Furthermore, induced SOX21 expression in pre-established GBM reduces tumor growth and significantly extends the survival of orthotopically transplanted mice. SOX21 acts as a tumor suppressor by binding to and epigenetically repressing AP-1-targeted chromatin, thereby downregulating adjacent genes. Consistently, the anti-tumorigenic activities of SOX21 are replicated by small molecules that inhibit AP-1 activity, whereas overexpression of an AP-1 transcription factor reverses these effects. Overall, this research demonstrates the potent role of SOX21 in restricting GBM progression through repression of AP-1-stimulated tumor-promoting gene expression.

Introduction

GBM is the most frequent and aggressive form of primary brain tumors[1]. It is characterized by uncontrolled growth, cellular and molecular heterogeneity, and a high propensity for recurrence. One major reason why conventional therapies unavoidably fail is explained by the presence of treatment-resistant GSCs[2]. These cells exhibit extensive self-renewing capacity, supporting rapid tumor growth and high cellular plasticity, which creates inter- and intra-tumoral diversification[2,3]. Furthermore, their tumor-initiating potential[4] underscores the need for novel strategies to target GSCs to counteract GBM progression and recurrence.

Transcription factors that promote the growth of healthy stem cells, such as members of the *SOX*, *POU*, *AP-1*, *GLI* and *E2F* families, have been shown to possess oncogenic functions in GSCs[5–10]. For instance, while the HMG-box transcription factor SOX2 is a vital regulator of stem cells in various developing and adult tissues, it is also necessary for GSC propagation and their tumor-inducing capacity[11,12]. Similarly, AP-1 transcription factors, which have ubiquitous roles in regulating cell proliferation and survival[13], also promote stem cell-like properties and aggressiveness of GSCs[8,9]. In contrast, the transcription factor SOX21 exhibit the opposite activity and reduces neural stem cell proliferation and promotes their differentiation[14]. Interestingly, in glioma, the expression level of SOX21 is negatively correlated with malignancy grade, such that SOX21 expression is significantly decreased in high-grade glioma samples compared to those of low-grade[15]. Consistent with this, exogenous expression of SOX21 in human GSCs diminishes their ability to form secondary tumors following orthotopic transplantation into mice[15,16]. Conversely, genetic ablation of SOX21 strongly increases the propensity of mouse brain stem cells to induce GBM-like tumors in an H-RAS/AKT-driven

glioma model[15]. These loss-of-function experiments indicate that SOX21 prevents malignant proliferation of neural stem cells exposed to oncogenic insults by facilitating the upregulation of cyclin-dependent kinase inhibitors, including CDKN1A and CDKN1B[15]. Although these findings underscore the capacity of SOX21 in preventing oncogenic transformation of brain stem cells and blocking the tumor-initiating capacity of GSCs, it is in a therapeutic perspective important to examine if SOX21 can inhibit the propagation of GSCs residing in an established, growing GBM. Moreover, to understand how SOX21 acts as a tumor suppressor, it is critical to elucidate the mechanisms by which SOX21 counteracts genetic pathways that preserve GSC properties and promote tumor progression.

In this study, we generated an inducible expression system in patient-derived GSCs and demonstrate that the induction of SOX21 expression can counteract the progression of pre-established GBM and thereby improve the survival rate of orthotopically transplanted mice. Our work provides evidence of how SOX21 achieves its tumor-suppressor function in GSCs, notably through the repression of tumor-promoting gene expression activated by AP-1 transcription factors.

Results

SOX21 expression in GBM is confined to stem and progenitor cells and has a prognostic value for patient survival.

To address the role of SOX21 in high-grade glioma we initially examined its expression pattern across GBM surgical samples (WHO grade IV, IDH wild type) using immunofluorescence. In these tumors, the vast majority of the SOX21^{+} cells expressed SOX2 (Fig. 1a-c, g; Supplementary Fig. 1a-d) and SOX21 expression could be detected in most self-renewing KI67^{+} cells (Fig. 1d-g; Supplementary Fig. 1a-d). These findings indicate that SOX21 expression in GBM is mainly confined to stem and progenitor cells.

Considering the inverse relationship between SOX21 expression levels and glioma malignancy grades (grade II/III vs. grade IV glioma), which we previously documented[15] we aimed to determine the prognostic significance of *SOX21* expression levels in GBM for patient survival. To address this issue, we divided the GBM mRNA data sets from "The Cancer Genome Atlas" (TCGA) into two groups, based on *SOX21* levels, and correlated these to the patient survival. Notably, Kaplan-Meier survival analyses revealed that patients with GBM exhibiting higher *SOX21* expression demonstrated significantly better Disease-Specific Survival (DSS), compared to those with lower *SOX21* expression levels (Fig. 1h). Furthermore, this correlation was present across different transcriptional subtypes of GBM (Supplementary Fig. 1e-h), underscoring the prognostic value of *SOX21* expression levels.

Elevated levels of SOX21 inhibit the proliferation and survival of GSCs.

The positive correlation between *SOX21* expression levels in GBM and patient survival rates, imply that high levels of SOX21 could exert an anti-tumorigenic activity in high-grade glioma. To address this possibility, we generated a tetracyclin-inducible (TetOn) lentiviral system harboring a Flag-tagged version of *SOX21* (*pLVX-SOX21*) and, as a control, a version lacking insert (*pLVX*) (Fig. 2a). The resulting viruses where stably transduced into primary GSCs derived from three different GBM tumors; GSCs that we from now on refer to as JM11, JM12, and JM13. In comparison to previously published glioma subtype transcriptional signatures[9,17,18], RNA-seq analysis revealed that these GSCs were best classified as classical (JM11), proneural (JM12), and mesenchymal (JM13) subtypes, respectively (Supplementary Fig. 2). Following selection for successfully transduced cells, the expanded GSCs were confirmed, with immunoblotting and immunofluorescence analyses, to specifically upregulate SOX21 upon doxycycline (DOX) treatment (Fig. 2b; Supplementary Fig. 3a, b).

In comparison to control GSCs (*pLVX*+DOX and *pLVX-SOX21*), DOX-induced expression of SOX21 (*pLVX-SOX21*+DOX) rapidly reduced the density of GSCs in monolayer cultures (Fig. 2c) and reduced the proportion of GSCs undergoing active proliferation, as evidenced by the incorporation of the thymidine analog EdU (Fig. 2d). Furthermore, flow cytometry (FACS) based analysis of AnnexinV expression and propidium iodide labeling revealed that induced SOX21 expression induced a significant increase in the proportion of early and late apoptotic GSCs (Fig. 2e-h). We further examined the impact of SOX21 on the clonal expansion capabilities of GSCs. Within 5-7 days of culture, DOX-induced expression of SOX21 resulted in a notable reduction in the number and size of the tumor spheres formed, compared to controls (Fig. 2i-l). Thus, increased levels of SOX21 reduce GSC proliferation, survival, and clonal expansion potential.

Induced SOX21 expression reduces GBM growth in orthotopic mouse models.

To further evaluate the anti-tumorigenic effects of SOX21, we investigated its capability to restrict GBM growth. Previous studies have demonstrated that viral-mediated expression of SOX21 in GSCs and glioma cell lines inhibits their capacity to induce tumor formation in orthotopic mouse models[15,16]. However, from a therapeutic perspective, examining if the induction of SOX21 in established GBM can counteract further tumor growth, is important. To address this issue, we transplanted GSCs of different origins (JM11, JM12, and JM13), engineered with DOX-inducible SOX21 expression or control systems, along with a constitutive lentiviral Luciferase (Luc) reporter, into the striatum of NOD-SCID mice (Fig. 3a). Serving as a control, we also transplanted mice with Luc-expressing GSCs additionally transduced with a DOX-activated SOX2 expression system (*pLVX-SOX2*; Supplementary Fig 3c). After that tumor establishment was confirmed via luciferase activity measurements, using an *in vivo* imaging system (IVIS), mice were provided with DOX-supplemented food to induce transgenic expression[19] (Fig. 3a-c). Bioluminescent imaging every two weeks revealed that SOX21 induction (*pLVX-SOX21*+DOX) significantly reduced further GBM growth compared to control tumors (*pLVX*+DOX and *pLVX-SOX21*) (Fig. 3d, e). The suppression of tumor growth in response to SOX21 induction was further reflected by the significantly prolonged mean survival time of mice, compared to mice with control tumors (Fig. 3f, g; Supplementary Fig. 4a). In contrast, DOX-induced expression of SOX2 did not affect tumor growth or significantly alter the mean survival rates of the transplanted mice (Fig. 3h-j; Supplementary Fig. 4b-d). Thus, induced expression of SOX21, unlike that of SOX2, in pre-established GBM can reduce continued tumor growth.

Despite the suppression of tumor growth in response to SOX21 induction, hematoxylin and eosin (H&E) staining showed no significant differences in the final sizes between end-point tumors across the different groups (Fig. 4a, b; Supplementary Fig. 5a, b). To determine the transgenic activity in end-point tumors we examined the presence of DOX-induced SOX21 expression using FLAG and SOX21 antibodies. While many tumoral cells co-expressed these markers we could detect tumoral regions, especially in GBM originating from GSCs JM11, which lacked transgenic SOX21 expression (Fig. 4c, d; Supplementary Fig. 5c, d). Nevertheless, induction of exogenous SOX21 expression in GBM resulted in a significant decrease in the proportion of cells expressing the proliferation marker KI67 and the stem cell marker SOX2 (Fig. 4c-f; Supplementary Fig. 5c-f). Thus, the decreased GBM growth detected after DOX-induced SOX21 expression coincides with a reduction of mitotically active GSCs.

SOX21 binds and represses tumor-promoting genes in GSCs.

To gain molecular insights into how SOX21 inhibits glioma progression, we next examined what genes SOX21 binds and regulates in GSCs, using SOX2 as a control. We explored this issue utilizing RNA-sequencing (RNA-seq) and chromatin immunoprecipitation combined with deep-sequencing (ChIP-seq) analyses of two GSC lines (JM11 and JM13). In comparison to controls, induced SOX21 expression for 48 hours deregulated more than a thousand genes (Fig. 5a, b; Supplementary Fig. 6a, b). Notably, among the most significantly increased genes was *CDKN1A*, which encodes the tumor suppressor p21 (Fig. 5a, b; Supplementary Fig. 6a-c). SOX21 expression also led to an upregulation of gene sets linked to the gene ontology (GO) terms "*neuron apoptotic process"*, *glial cell apoptotic process*" and "*negative regulation of cell cycle process*" (Fig. 5c; Supplementary Fig. 6d). Conversely, genes that have been implicated in glioma progression, including *CDK6*, *EFNB2*, *HDAC9,* and *SOX2* were among those

significantly downregulated (Fig.5a, b; Supplementary fig. 6a, b)[20–24]. SOX21 expression also led to the downregulation of gene sets linked to the GO-terms "*Positive regulation of cell cycle process*" (Fig. 5c; Supplementary fig. 6d), as well as "*Cell adhesion*", "*Response to growth factors*", "*Mitotic cell cycle*" and "*MAPK cascade*" (Supplementary Fig. 6e). SOX2 overexpression deregulated genes that were distinct from those altered by SOX21 (Supplementary Fig. 6f-i), but notably reduced the cell cycle gene *CCND1*[25] (Supplementary Fig.6f, g). Together, these findings underscore the role of SOX21 in promoting a gene expression profile in GSCs that opposes tumor progression.

The ChIP-seq experiments showed a high degree of consistency across replicates (Supplementary Fig. 7a-c). These experiments identified thousands of binding sites (peaks) for both SOX21 and SOX2 (Fig. 5d-f), with a SOX binding sequence as the most centrally enriched motif (Fig. 5g, h; Supplementary Fig. 7a, b). Notably, approximately one-third of the genomic regions targeted by SOX21 were consistent across both lines of GSCs (JM11 and JM13) (Fig. 5d). However, the overlap in binding sites between SOX21 and SOX2 was less than 10% (Fig. 5e, f). Interestingly, centrally enriched motif analysis also revealed a significant enrichment of AP-1 transcription factor binding sites in SOX21 bound regions (Fig. 5g; Supplementary Fig. 7d), an enrichment that could not be explained by cross reactivity of the antibodies used in the ChIP-seq experiments (Supplementary Fig. 7f, g). No enrichment of AP-1 binding sites could be detected in regions bound by SOX2 (Fig. 5h; Supplementary Fig. 7e). By analyzing SOX21 peak regions we identified a strong enrichment of SOX and AP-1 motifs spaced between 1-2 base pairs (Fig. 5i; Supplementary Fig. 7h). A similar analysis of SOX2 targeted chromatin regions revealed strong enrichment of SOX and POU binding sites, spaced between 2-3 base pairs (Fig. 5j; Supplementary Fig. 7i). Moreover, while SOX21 binding was strongly

associated with SOX21 suppressed genes (closest transcriptional start sites) (Fig. 5k), SOX2 binding was predominately associated with genes activated by its overexpression (Fig. 5k). Hence, SOX21, but not SOX2, represses genes in GSCs by binding to genomic regions in close proximity to AP-1 motifs.

SOX21 binds and reduces the accessibility of AP-1 targeted chromatin regions.

The observation that SOX21 represses rather than activates gene expression in GSCs raises the question regarding the underlying molecular mechanisms. To address this, we explored the impact of induced SOX21 expression for 48 hours, on the accessibility of SOX21-bound chromatin in GSCs (JM11). This was achieved through the "Assay for Transposase-Accessible Chromatin using sequencing" (ATAC-seq)[26]. Quality control measures verified the reliability and reproducibility of the different ATAC-seq experiments (Supplementary Fig. 8a-d). Principal component analysis of ATAC-seq data showed that DOX-induced expression of SOX21, but not DOX alone, markedly altered the chromatin architecture compared to controls (Supplementary Fig. 8b). These experiments identified approximately 50 000 chromatin regions that exhibited altered accessibility in response to SOX21 activation, with nearly equal numbers showing either an increase or decrease in ATAC-seq signals (Fig. 6a). Of the chromatin areas targeted by SOX21 (6707 SOX21 ChIP-seq peaks in JM11) approximately 60% showed changes in their accessibility following SOX21 induction. To assess the significance of these chromatin alterations on gene expression, we examined the expression of the adjacent genes after SOX21 induction. This analysis revealed a significant enrichment of chromatin regions with reduced accessibility around genes that are downregulated by SOX21 (Fig. 6b). In contrast, chromatin regions with increased accessibility were associated with both repressed

and activated genes (Fig. 6b). Thus, SOX21-repressed genes are best predicted by their association with chromatin regions that are condensed upon SOX21 binding.

To better understand how these condensed chromatin regions can contribute to SOX21-mediated gene repression we next evaluated their association with the epigenetic markers H3K27ac and H3K4me1; indicative of primed and potentially active enhancers[27,28]. ChIP-seq experiments on GSCs (*pLVX-SOX21*), cultured with or without DOX, revealed a strong reduction in H3K27ac and H3K4me1 levels at chromatin regions that are bound by SOX21 (Fig. 6c-f; Supplementary Fig. 9a-e). Moreover, HOMER analysis identified significant enrichment of AP-1 and SOX binding motifs in these chromatin regions, in comparison with condensed chromatin areas that are not targeted by SOX21 (Fig. 6g; Supplementary Fig. 9f). To examine the transcription factor activity at the AP-1 and SOX binding motifs we used ATAC-seq data to perform genomic footprint experiments. Interestingly, we found that robust AP-1 footprints strongly correlated to chromatin regions targeted by SOX21, but that their presence was independent of induced SOX21 expression (Fig. 6h and i; Supplementary Fig. 9g and h). In line with this relationship, significant SOX footprints were identified in chromatin with robust AP-1 footprints, but only in the presence of exogenous SOX21 expression (Fig. 6h and i). These findings indicate that SOX21 inhibits tumor-promoting gene expression in GSCs by binding to and repressing chromatin targeted by AP-1 transcription factors.

Pharmacological inhibition of AP-1 mimics SOX21 function in GSCs.

Given the central role of AP-1 transcription factors in maintaining and progressing various types of cancer stem cells, we next examined the gene regulatory convergence of SOX21 and AP-1. To this end, we analyzed the gene expression patterns in two GSC lines, JM11 and JM13,

after pharmacological inhibition of AP-1, using the small molecules T-5224[29] and SR 11302[30,31]. By comparing gene expression alterations following AP-1 inhibition with those altered by SOX21, we observed a strong concordance among genes suppressed, though not among genes activated. This correlation was highly significant for both AP-1 inhibitors across both GSC variants (Fig. 7a; Supplementary Fig. 10a). Correspondingly, genes downregulated by T-5224 and SR 13022 treatment were linked to GO-terms also negatively regulated by SOX21, such as those related to "*Mitotic cell cycle"* and "*Cell adhesion"* (Fig. 7b; Supplementary Fig. 10b).

To investigate how the pharmacological inhibition of AP-1 transcription factors affects GSCs, we analyzed the survival, proliferation, and sphere-forming capacity of GSCs cultured with T-5224 and SR 11302. Inhibition of AP-1 function resulted in a significant reduction in viable cell counts (Fig. 7c and d; Supplementary Fig. 10c and d), alongside a strong suppression of actively dividing cells, as examined by the incorporation of EdU (Fig. 7e; Supplementary Fig. 10e). Moreover, treatment with AP-1 inhibitors impaired the ability of GSCs to form and grow as tumor spheres (Fig. 7f-h; Supplementary Fig. 10f-h). Thus, inhibition of AP-1 function mimics the activity of induced SOX21 expression in GSCs. Conversely, increasing the level of AP-1, through c-JUN overexpression, effectively counteracted the reduction in cell viability and proliferation in response to SOX21 induction (Supplementary Fig. 10i and j). Taken together, these experiments underscore a tumor suppressor function of SOX21 by reducing GSC survival, proliferation, and oncogenic potential via the repression of AP-1.

Discussion

The prevailing treatment protocol for GBM involves surgery, radiation, and chemotherapy using DNA-alkylating agents[32]. However, this treatment strategy often fails due to its inability to eradicate treatment-resistant GSCs. Therefore, the development of innovative treatments that simultaneously target both the bulk tumor cells and GSCs is critically needed.

Previous loss-of-function studies in mice have demonstrated that SOX21 is necessary to prevent malignant transformation of brain neural stem cells exposed to an oncogenic insult[15]. Moreover, experiments in which SOX21 is overexpressed in primary human GSCs before transplantation into mice highlight the potential of SOX21 to inhibit their tumor-initiating capacity[15,16]. While these results align with the tumor suppressor function of SOX21 their therapeutic relevance can be questioned. By generating patient-derived GSCs, equipped with an inducible SOX21 expression system, we have in this study demonstrated the ability of SOX21 to impede tumor progression upon its induced expression in established GBM, which ultimately leads to an extended survival of the orthotopically transplanted mice. Our findings reveal a negative association between SOX21 expression levels and GSC self-renewal and survival. Notably, the reduction in GSC properties following DOX-induced SOX21 expression was accompanied by a significant decrease in the expression of GSC-related genes such as *SOX2*, *HDAC9*, *CDK6,* and *EFNB2*, which are known to facilitate glioblastoma growth[20–24].

A key finding of this study is that SOX21 mediates its tumor suppressor function by repressing the activity of the AP-1 transcriptional complexes, which have well-established functions in promoting cancer stem cell properties and aggressiveness, sustaining tumor growth and contributing to treatment resistance[9,33,34]. This conclusion is supported by the observation that SOX21 shows a strong preference for SOX binding sites in close proximity to targeted AP-

1 motifs. Moreover, pharmacological inhibition of AP-1 in GSCs mirrors the activity of induced SOX21 expression both in the regulation of downstream genetic pathways, and in affecting GSC proliferation, viability, and tumor-sphere forming capacity. Interestingly, while high SOX21 expression levels correlate with improved GBM patient outcomes, elevated levels of AP-1 transcription factors generally predict poorer prognosis[9]. Consistently, AP-1 transcription factors have been implicated in regulating GBM subtype plasticity and their transition into a mesenchymal-like state[8,9,35], often associated with recurrence and worse patient outcomes[17]. Further investigation is needed to understand how SOX21 counteracts AP-1 function in GSCs. However, it is noteworthy that while SOX21 can reduce the accessibility of targeted DNA regions, AP-1 transcription factors can promote chromatin opening through an interaction with the SWI/SNF chromatin remodeling complex[34,36,37], a function that can contribute to tumor initiation[34]. Taken together, these findings provide significant insights into how SOX21 reduces GSCs properties and GBM aggressiveness through its capacity to repress the tumor-promoting activity of AP-1 transcription factors.

In contrast to SOX21, SOX2 has been referred to as an oncogene due to its necessity for the maintenance and expansion of various types of cancer stem cells [11,24,38–42]. In glioma, elevated levels of SOX2 have been linked with increased tumor aggressiveness and poorer patient prognosis[43]. Even though the induced SOX2 expression experiments presented in this study did not alter the growth pattern of the GBM, knock-down studies have previously demonstrated the requirement of SOX2 for GSC proliferation and tumor-inducing capacity[23,24]. The DNA-binding HMG domains of SOX21 and SOX2 are highly conserved, but while the C-terminal domain of SOX21 acts as a transcriptional repressor, that of SOX2 functions to activate transcription[44]. Interestingly, a SOX2 version, with an intact HMG

domain, engineered to function as an epigenetic repressor has a similar activity as SOX21 and can counteract GBM growth after its local, viral-based delivery into mouse brains[45]. Although one interpretation of these findings aligns with the previous idea that SOX21 and SOX2 act on a shared set of target genes[14,46], we found a surprisingly limited target site overlap (< 10%) in GSCs. Consequently, induced SOX21 expression regulated an insignificant fraction of the SOX2-bound genes in GSCs. One explanation for the divergent binding pattern of SOX21 and SOX2 is that the target selection of SOX proteins is generally dependent on their collaboration with partner transcription factors[46]. Here we demonstrated that while SOX21 binds DNA in the vicinity of AP-1 targeted motifs, SOX2 binding is enriched around motifs for POU transcription factors, which are well-established partner factors of SOX2 in different stem cell compartments[46–49]. Thus, although SOX21 and SOX2 inversely regulate similar processes in GSCs, their different binding patterns and cooperation with unique partner factors indicate that they achieve these effects by controlling distinct molecular pathways.

This study not only reveals that the tumor-suppressive role of SOX21 in GBM is dependent on the repression of AP-1 target genes, but also demonstrates that the modulation of its activity constitutes a potential therapeutic strategy. While direct pharmacological activation of SOX21 could be challenging, targeting associated or downstream molecular pathways offers a promising alternative. By elucidating the mechanisms through which SOX21 controls glioma biology, we have provided insights that could be critical in developing novel strategies to target GSCs.

Figure legends

Fig. 1 Prognostic Relevance of SO21 expression in GBM Patient Survival. a-c Immunofluorescent staining of a GBM surgical sample (GBM1409) showing SOX21 protein localization (green in **a** and **c**) predominately in $SOX2^+$ cells (red in **b** and **c**). Insets represent magnified views of the tumor area. **d-f** SOX21 expression (green in **d** and **f**) can be detected in most actively proliferating, $KI67^+$ cells (red in **e** and **f**). **g** Statistical co-expression analysis of SOX21, SOX2 and KI67 proteins in GBM sample (GBM1409). **h** Kaplan-Meier survival curves based on TCGA GBM mRNA expression profiles (n=152 samples) show significantly better ($p=2x10^{-6}$) disease-free survival with high SOX21 expression (red line) compared to low expression (blue line). Scale bar corresponds to 50 µm in (**a**-**c)** and 30 µm in (**d**-**f)**.

Fig. 2 Effects of Inducible SOX21 Expression on GSC Growth. a Schematic drawing of the tetracycline-controlled (Tet-On) SOX21 expression system. rtTA, tetracycline-controlled transactivator; TRE, Tet response elements; DOX, doxycycline. **b** Western blot analysis showing Flag-tagged SOX21 protein levels in GSCs (JM11 and JM13) with either a control (*pLVX*) or inducible SOX21 expression system (*pLVX-SOX21*), cultured with or without DOX for 48 hours. **c** DOX-induced SOX21 expression reduces the density of GSC monolayer cultures. **d** Statistics of EdU incorporation in control and SOX21 expressing GSCs (JM11 and JM13). **e** and **f** Flow cytometry analysis of GSCs (**e**, JM11; **f**, JM13) with *pLVX* or *pLVX-SOX21*, cultured with or without DOX for 4 days. Q1 represents live cells; Q2, early apoptotic cells; Q3, late apoptotic cells; Q4, necrotic cells. **g** and **h** Quantitative results from flow cytometry experiments showing increased apoptosis in GSCs following DOX-induced SOX21 expression, assayed by Annexin V labeling. **i** and **j** Representative images showing the sphere-forming capacity of GSCs (**i**, JM11; **j**, JM13) harboring control and SOX21 expression systems. **k** and **l** Bar graphs represent the

number and size of spheroids formed under each experimental condition by JM11 (**k**) and JM13 (**l**). Scale bars correspond to 70 µm in (**c**) and 500 µm in (**i** and **j)**.

Fig. 3 Induced SOX21 Expression Hinders Growth of Pre-Established GBM in Mouse Models. **a** Experimental setup for assessing the impact of inducible SOX21 expression on pre-established GBM in mice, using luciferase tracking for the visualization of tumor growth. **b** and **c** Bioluminescence imaging showing initial tumor establishment in mice transplanted with control or SOX21 inducible GSCs (**b**, JM13; **c**, JM11). **d** and **e** Graphs depicting tumor growth after that transplanted mice (**d**, JM13; **e**, JM11) were supplemented with control or DOX-containing food. The tumor burden, as represented on the Y-axis, was quantified by luciferase intensity. **f** and **g** Kaplan-Meier survival analysis of transplanted mice (**f**, JM13; **g**, JM11) after that transplanted mice were supplemented with control or DOX-containing food. The data shows significantly extended survival with SOX21 induction. **h** Bioluminescent evidence of tumor establishment in mice transplanted with GSCs (JM11) harboring a control (*pLVX*) or an inducible SOX2 expression system (*pLVX-SOX2*). **i** Graph depicting tumor growth after that transplanted mice were supplemented with control or DOX-containing food. **j** Kaplan-Meier survival analysis of mice post-DOX treatment.

Fig. 4 Histopathological Analysis and Marker Expression in End-State Tumors. **a** and **b** Representative H&E images of end-state tumors formed in DOX-treated mice transplanted with GSCs (JM13) harboring a control (*pLVX*) (**a**) or inducible SOX21 expression system (*pLVX-SOX21*) (**b**). **c** and **d** Close-up images of the tumors (insets in **a** and **b**) are showing immunohistochemical analysis for human nuclei (HuNu), FLAG-tagged SOX21, SOX21, SOX2, and the proliferation marker KI67. **e** and **f** Quantification of KI67 and SOX2 expression in

control and SOX21 expressing GBM. Scale bars correspond to 1 mm in (**a),** 1,5 mm in (**b**) and 75 µm in (**c** and **d)**.

Fig. 5 Transcriptomic Impact of SOX21 Expression in GSCs. a and **b** Volcano plots showing differential gene expression in GSCs, JM11 (**a**) and JM13 (**b**), after DOX-induced SOX21 expression for 48 hours. Genes significantly upregulated in comparison with control cells (*pLVX-SOX21*) are represented with red dots and genes significantly downregulated with blue dots (false discovery rate $<$ 0,01). **c** Heatmaps show gene sets and their linked GO-terms deregulated in GSCs upon DOX-induced SOX21 expression. **d-f** Venn diagrams comparing SOX21 and SOX2 ChIP-seq peak regions in GSCs (JM11 and JM13). The peak numbers represent targeted regions identified in each of 3 independent replicate experiments. **g** and **h** Enrichment of SOX motifs (red line) and AP-1 motifs (blue line) and their distances to the center of SOX21 (**g**) and SOX2 (**h**) peaks identified by ChIP-seq experiments conducted in GSCs JM11. P-values of best-matching SOX and AP-1 motifs are shown. Distances are given in base-pairs (bp). **i** and **j** Graphs depict the most significant distances between centrally enriched SOX motifs and AP-1 motifs in SOX21 ChIP-seq peaks (**i**) and POU motifs in SOX2 ChIP-seq peaks (**j**) in GSCs JM11. The gap between motifs is based on the bp spacing between the last nucleotide in the SOX motif and the first nucleotide in AP-1 (**i**) or POU (**j**) motifs. **k** Bar graph showing the gene expression differences of SOX21 and SOX2 bound genes after DOX-induced SOX21 and SOX2 expression, quantified by p-values and compared with non-DOX conditions.

Fig. 6 SOX21 Binding and Repression of AP-1 targeted genes. a MA-plot showing changes in chromatin accessibility, identified by ATAC-seq, after 48 hours of DOX-induced SOX21 expression (*pLVX-SOX21*+DOX). Regions significantly increased and decreased in their

accessibility compared to control cells (*pLVX-SOX21*) are marked with blue dots (false discovery rate < 0,05). **b** Bar graph showing the correlation between SOX21 induced changes in gene expression and chromatin accessibility at SOX21 ChIP-seq peak regions. **c-e** The read mean density of ATAC-seq (**c**), H3K27ac (**d**), and H3K4me1 (**e**) ChIP-seq peaks in control (red line) versus SOX21 induced (blue line) GSCs. **f** Read density tracks show representative examples of SOX21 ChIP-seq (grey), ATAC-seq (green), H3K27ac (red), and H3K4me1 (blue) ChIP-seq peaks found in control or DOX-induced SOX21 expressing GSCs. **g** Statistical enrichment of transcription factor binding motifs in condensed chromatin regions overlapping with SOX21 ChIP-seq peaks. P-values correspond to the enrichment of motifs compared to that in condensed DNA regions that do not overlap with SOX21 binding. **h** and **i** Footprint analysis of ATAC-seq data at AP-1 and SOX motifs, present in chromatin regions that become condensed upon DOX-induced SOX21 expression. Chromatin regions that do not overlap with SOX21 ChIP-seq peaks (**h**) are compared to chromatin regions that overlap with SOX21 ChIP-seq peaks (**i**). Mean aggregate ATAC-seq signals are shown on y-axes and the number of analyzed motifs is stated in graphs.

Fig. 7 Comparative Effects of AP-1 Inhibitors and SOX21 on Gene Expression in GSCs. a RNA-seq analysis comparing the gene regulatory effects of AP-1 inhibitors (T-5224 and SR 11302) and SOX21 in GSCs (JM11) reveals a significant overlap between genes suppressed, but not among genes activated. **b** GO-term enrichment of genes regulated by AP-1 inhibitors. Dark bars correspond to genes deregulated in GSCs by SR 11302 and grey bars correspond to genes deregulated by T-5224. Enrichments are presented as Bonferroni-adjusted q-values. **c** Images of GSCs treated with DMSO (control), T-5224, or SR 11302 for 4 days. **d** and **e** Quantitative assessments of cell viability (**d**) and proliferation (EdU incorporation) (**e**) in response to the

treatment with T-5224 or SR 11302. **f** Representative images show the sphere-forming capacity of GSCs (JM11) treated with DMSO (control), T-5224, or SR 11302. **g** and **h** Quantitative assessments of numbers and sizes of spheres formed in the presence of DMSO, T-5224, or SR 11302. **i** Overexpression of c-JUN in GSCs did not alter the number of live cells after 48 hours but prevented the cell reduction caused by DOX-induced SOX21 expression. **j** Bar graph represents a quantitative assessment of the viability of GSCs after overexpressing c-JUN for 48 hours, in the presence or absence of DOX-induced SOX21 expression. Scale bars correspond to 50 µm in (**c**) and 400 µm in (**f**).

Materials and Methods

SOX21 expressing GSCs

Human glioblastoma (GBM) tissue samples and primary GBM cell cultures were obtained from the Karolinska Institute Biobank (Karolinska Hospital) under ethical permit number 2023-01366-01. These primary GBM cell lines, established according to a previously described protocol[15], were cultured on poly-L-ornithine and Laminin (Sigma-Aldrich) coated plates. The culture medium used was Human NeuroCult NS-A Proliferation media (Stem Cell Technology) supplemented with 2 µg/mL heparin (Stem Cell Technology), 10 ng/mL FGF (Stem Cell Technology), 20 ng/mL EGF (Stem Cell Technology), and penicillin/streptomycin (Gibco).

To induce SOX21 and SOX2 expression, primary GBM cell lines were transduced with DOX-regulated lentivirus (*pLVX-SOX21*, *pLVX-SOX2*, or *pLVX*). The medium was supplemented with 6 µg/mL Puromycin for 4 weeks to select for transduced cells. For *in vivo* experiments, cells were further transduced with a lentivirus encoding constitutively active Luciferase (*pGK-Luc*) without additional antibiotic selection before grafting into mice. All primary cells were used at passages below 10 and were regularly tested for mycoplasma using the MycoAlert Mycoplasma Detection kit (Lonza). For the onset of transgenic expression cells were treated with 200 ng/mL DOX for 48 hours before being subjected to downstream assays unless otherwise specified.

Intracranial transplantation of GSCs

All animal experiments were conducted in compliance with Swedish animal welfare laws and authorized by the Stockholm Animal Ethics Committee (Dnr 3696-2020). A suspension of human GBM

cells was prepared at a concentration of 50,000 cells per microliter, with a viability of at least 80%. The cells were kept on ice up to two hours after harvesting. 150,000 cells were stereotactical injected (3 microliters) into the striatum of NOD.CB17-PrkcSCID/J mice, aged 6-10 weeks. The coordinates for injection relative to bregma were 2.0 mm lateral, 1.0 mm anterior, and 2.5 mm deep. During the procedure, mice received pre-operative analgesics subcutaneously 0.1 mg Norocarp/Carprofen (2-5 mg/kg) and were anesthetized with isoflurane during the transplantation procedure. Local analgesia was achieved at the incision site using Marcain (2.5 mg/ml). Post-operative care included subcutaneously administering of 0.001 mg Temgesic/Vetergesic (0.05-1 mg/kg), and monitoring recovery in a heated cage. Mice were checked daily for one week and received analgesics for two days post-surgery. Animal health was monitored daily using a scoring system based on physical and behavioral criteria following the Karolinska Institutet animal facility guidelines. Mice exhibiting/showing symptoms of distress and unhealthy behavior were euthanized according to guidelines stipulated in the ethical permit. Survival data were recorded for statistical analysis.

In vivo bioluminescence imaging

Tumor growth was monitored using an IVIS Spectrum CT Preclinical In Vivo Imaging System (Perkin Elmer). Mice were injected intraperitoneally with 150 mg/kg of D-Luciferin and imaged 23 minutes post-injection to capture peak luminescence. During image acquisition, the animals were maintained at 37°C and under gaseous anesthesia (2–3% isoflurane and 1 lt/min O2). Images were analyzed using Living Image software (Version 4.5.2.18424, Perkin Elmer) to assess the bioluminescence intensity in specific regions of interest (ROI). The animal's weight was checked before the IVIS measurement.

Perfusion and ex-vivo sample processing

Unhealthy mice were deeply anesthetized with an intraperitoneal injection of a ketamine/xylazine mixture. Transcardial perfusion was performed with phosphate-buffered saline (PBS) followed by 4% paraformaldehyde (PFA) in PBS[50]. The brains were carefully extracted from the skull, post-fixed in 4% PFA, and sectioned on a coronal cut approximately near bregma using a mouse brain matrix. Tissue samples were processed for both cryopreservation in OCT and paraffin. The OCT brains were cut coronally in 15 um sections on a cryostat (Cryotome Cryostar NX70 Thermo Scientific). For paraffin block processing, brain tissues after fixation, were dehydrated on a tissue processor Leica TP1020 and subsequentially embedded in paraffin. 5-um paraffin sections were prepared using an automated microtome HM355S.

Hematoxylin and eosin (H&E)

Hematoxylin and eosin staining was performed to visualize tumor morphology and pathology. Tissue sections of 5 µm thickness were prepared and underwent deparaffination treatment followed by hydration using ethanol solutions and water. Mayers Hematoxylin and Eosin Y (eosin 0.2%, Histolab, article no. 01650) were used for staining. Stained sections were examined for glioblastoma histopathology features using a Nikon ECLIPSE E1000M microscope, and images were captured with a Zeiss AxioScan.Z1 Slide Scanner. Image analysis was performed using QuPath vs0.2.3 and ImageJ software.

Immunofluorescence

Tissue slides from mouse experiments underwent deparaffination through sequential incubations in xylene, ethanol, and water, followed by permeabilization with 1xPBS 1xPBS containing 0.3% Triton X-

100. Antigen retrieval was performed by boiling the slides in DAKO antigen retrieval buffer whereafter sections were blocked for 1 hour at room temperature with a solution containing 4% donkey serum/FBS in 0.1% Triton X-100 in 1xPBS. Slides were incubated overnight at room temperature with primary antibodies diluted in binding buffer (4% donkey/FBS in 0.1%Triton X-100 in 1xPBS). After washing and incubation with secondary antibodies, slides were mounted in a Fluorescence Mounting Medium (DAKO). Images were captured with confocal microscope ZEISS LSM700. For antibody staining of fresh frozen human GBM tissues, sections of untreated tumor tissue were fixed in 2% Formaldehyde at room temperature for 5 minutes, followed by three washes in PBS. Antibodies were diluted in PBS with 0.1% Triton-X and 1% FBS. Immunofluorescence analysis involved capturing three random images from each sample to quantify the number of positive nuclei for each marker using ImageJ software. DAPI was employed as a counterstain to visualize all nuclei.

Statistical analysis

Data were analyzed using GraphPad Prism (GraphPad Software, version 9.0.0, La Jolla, CA). Statistical significance was determined using unpaired t-tests or one-way ANOVA. Kaplan-Meier survival curves were compared by using the log-rank Mantel-Cox. For all comparisons, a p-value of less than 0.05 was considered as significant. For enrichment analysis between different gene sets (from ChIP-seq and RNA-seq experiments) we calculated the hypergeometric distribution (phyper, R software) from 23´000 human genes in total. Graphs are presented as -Log10 p-value. For Sox-21 expression analysis in TCGA glioblastoma cohort, RNA sequencing data and overall survival of 151 patients with Glioblastoma, were downloaded from The Cancer Genome Atlas (TCGA) data portal[51] (TCGA; https://cancergenome.nih.gov/). The cut-off value for *SOX21* mRNA expression was determined based on its median value. The relationship between *SOX21* mRNA expression and overall survival was

analyzed using the log-rank test with R software (version 4.3.1; R Foundation for Statistical Computing, Vienna, Austria)[52].

Neurosphere formation assay

Neurosphere formation assay was performed essentially as described in[15]. Primary GSCs were seeded at 10,000 per well in flat-bottom, low-attachment 24-well plates in DMEM/F12-Glutamax medium, supplemented with N2 supplement, B27, human recombinant EGF, bFGF (all from Stem Cell Technologies), 0.05% BSA, 1.5% FBS, L-Glu, and penicillin/streptomycin. Rock inhibitor/Y-27632 (STEMCELL Technologies, Cat #:72304) were added to the medium at the concentration of 1 uM to the first 1-2 days post-seeding. DOX (250 ng/ml) or AP-1 inhibitors (SR11302, Santa Cruz Biotechnology Cat #: sc-204295 at 10 uM concentration; T5224, Cayman Chemical, Cat #: 22904 at 100 uM of final concentration) were administered to designated wells, on day three, post-seeding. The culture medium was refreshed every two days. The assay was concluded after 10 days with DOX treatment and after 14 days with AP-1 inhibitors. Spheroid growth and morphology were assessed using a Leica CTR 4000 microscope and analyzed using ImageJ.

EdU assay, cell viability and apoptosis assay

GSCs were seeded at 100,000 cells per well in culture medium described above. DOX treatment started on day 1 post-seeding at a concentration of 200 ng/mL. The EdU assay was performed on day 2 post-DOX treatment, where cells were pulsed with 10 µM EdU on fresh medium without DOX for 3 hours. Following the EdU pulse, cells underwent Click-iT EdU staining according to the manufacturer's protocol (Click-iT EdU Flow Cytometry Assay Kits,

Invitrogen, Cat No. C10425). Flow cytometry analysis was conducted on a BD Canto II analyzer to assess the proliferation by evaluating 50,000 events per sample. Results were analyzed and plotted using GraphPad Prism software. For analysis of cellular apoptosis, cells were processed with the FITC Annexin V Apoptosis Detection Kit (BD Biosciences, 556547). Signal were analyzed by FACS (BD, FACSCanto II). Compensation was performed and all samples were made in triplicates. Data were analyzed by FlowJo™ software.

cJUN experiment

c-JUN used to counteract SOX21 activity in GSCs was ordered from addgene (34898) and sub-cloned into lentiviral vector pLVX-cJUN-IRES-mcherry. To examine it ability to counteract SOX21 activity, GSCs were seeded into 12-WD with around 60% confluence. DOX were added 5 hours before the virus were applied. DOX were refreshed every 2 days until the end of the experiment.

Western Blot Analysis.

Cultured cells were lysed using RIPA buffer (50 mM Tris, pH 8.0, 150 mM NaCl, 1% IGELPAL CA-630, 0.5% sodium deoxycholate, 0.1% SDS) supplemented with a protease inhibitor mixture (Roche, 04693116001). The lysates were rotated in a cold room for 10 min and cleared by centrifugation at 14,000 × g for 10 min at 4 °C. Protein concentration was determined by a Bradford Assay (Bio Rad, 500–0006). Loading buffer was added to the lysates, and an equal amount of protein was loaded on a gradient 8-12% SDS/PAGE gel together with a protein ladder (Pageruler, ThermoScientific, 26616). Subsequently, proteins were transferred to a nitrocellulose blotting membrane (Amersham 0.45 µm, 10600016) and blocked in 5% milk in PBS/0.1% Tween (Sigma, P1379) followed by primary antibody incubation overnight in a cold

room. Anti-mouse or anti-rabbit horseradish peroxidase-coupled secondary antibody (Vector Laboratories, WB-1000 WB-2000) was added in 1:5,000 dilution and incubated for 1 h. ECL immobilon western (Thermo, SuperSignal™ West Pico PLUS Chemiluminescent Substrate, 34580) was used as the chemical substrate.

Antibodies

Primary antibodies: Sox21 (R&D, AF3538, 1:150); SOX2 (Seven Hills Bioreagent, #WRAB-1236, 1:500); HuNu (Abcam, ab190710, 1:100); KI67 (ThermoFischer, 14-5698-82; 1:200 or Abcam, ab16667; 1:250); FLAG (Abcam, ab205606; 1:200). H3K27Ac (Diagenode, C15410174); H3K4me1 (Diagenode, C15410194). Secondary antibodies: Donkey anti-goat-488 (Alexa Fluor Invitrogen Ref A11055), Donkey anti-Rat-488 (Alexa Fluor Invitrogen Ref. A2120), Donkey-anti-rabbit 555 (Alexa Fluor Invitrogen Ref. A31572), Donkey anti-Mouse-555 (Alexa Fluor Invitrogen Ref. A31570), Donkey-anti-goat-555 (Alexa Fluor Invitrogen Ref. A21432), Donkey-anti-rabbit 488 (Alexa Fluor Invitrogen Ref. A21206).

ChIP-Seq

ChIP experiments were conducted following established protocols[53] using the following antibodies: goat anti-SOX21, rabbit anti-SOX2, rabbit anti-H3K4me1, and rabbit anti-H3K27Ac. ChIP libraries were prepared with the ThruPLEX® DNA-Seq Kit (Takara) and sequenced on the Illumina NovaSeq6000 SP-100 platform, producing paired-end 2x50bp or 2x150bp reads, generating >2 ×10^7 reads per ChIP experiment.

ChIP reads were aligned to the human genome assembly hg19 using Bowtie (version 1.3.1). Correlation plots between replicate BAM files were generated with deepTools/2.5.1. MACS2 was used for peak calling with default settings, except for SOX2 and SOX21 ChIP in JM13,

where an FDR of 0.001 was applied. Consensus peak sets were defined when signals were detected in all three replicates. Blacklisted regions from the human assembly hg19 (Encodeproject.org) were removed from the consensus peak sets. Centrally enriched motifs were identified using CentriMo[54], and the spacing between the most significant DNA-binding motifs was analyzed using SpaMo version 5.5.5 (default settings).

For H3K27Ac and H3K4me1 ChIP-seqs, reads were pooled from two replicates each. After removing duplicate reads, the pooled files were used without further processing. For comparison to ATAC-seq data (mapped to human genome assembly hg38), peak regions were transferred from hg19 to hg38 using LiftOver (UCSC, default settings), and mapped reads were transferred using CrossMap (version 0.6.6)[55]. Overlaps between ChIP-seq peaks were considered significant when >50% of peaks overlapped reciprocally, using the BEDTools intersect function. Overlaps between H3K27Ac and H3K4me1 ChIPs, SOX21 ChIP, and ATAC-seq were analyzed with seqMINER software[56], directly mapping reads from H3K27Ac-ChIP, H3K4me1-ChIP and ATAC-seq onto SOX21 peak regions.

Gene annotation was performed using GREAT 3.0.0[57]. Motif enrichment was analyzed with HOMER software[58] using the findMotifsGenome.pl function (default settings), with one peak set used as the background for the other in two individual HOMER runs.

ATAC-seq

Three replicates per experiment, with 50,000 cells per replicate, were used for Tn5-based ATAC experiments[58], performed by SciLife Lab Stockholm, Sweden, and DNA was sequenced on an Illumina NextSeq2000 to produce paired-end 2x50 bp reads. FastQ reads were

processed through the nf-core ATAC-seq bioinformatics pipeline (NGI, SciLife Lab Stockholm, Sweden, https://nf-co.re/atacseq/2.1.2) for mapping, quality control, peak calling, and peak annotation. Differences between ATAC peak sets were determined using DiffBind[59]. Footprint analysis was performed with Tobias[60] after correction of the Tn5 insertion bias (ATACorrect) and by using all open ATAC peaks in BINDetect and ScoreBigwig command for normalization of specific subsets of peaks from SOX21 ChIP-seq experiment (output peak sets).

RNA-seq

Approximately 200,000 cells per sample were harvested after 45-48 hours of DOX or no treatment. RNA was extracted using the Qiagen RNeasy Prep Kit following the manufacturers instructions. RNA-seq libraries were prepared with the TruSeq RNA Library Prep Kit v2 (Illumina) and sequenced on a NovoSeq6000 to produce 2x150 bp reads. FastQ files underwent demultiplexing, quality control, and mapping to the human genome assembly hg38 using the RNA-seq bioinformatics pipeline from NGI SciLife Lab (Stockholm, Sweden, https://nf-co.re/rnaseq/3.14.0). Differential gene expression analysis was performed using DESeq2[61], with significant genes identified by a log2 fold change < -1 or >1 and adjusted p-value < 0.05 for JM13 cells, and a log2 fold change of 0 with adjusted p-value < 0.05 for JM11 cells. Volcano plots illustrating gene expression changes post-DOX induced SOX21 or SOX2 expression were generated using the EnhancedVolcano R package[62]. Heatmaps of RNA-seq read counts for selected Gene Ontology (GO) gene sets were produced using the R function heatmap[52]. GO bar graphs were produced using ToppGene[63].

Data availability

Raw data fastq files from ChIP-seq, RNA-seq and ATAC-seq experiments (240 files) are available through the following link (BioProject ID: PRJNA1128363):

https://eur01.safelinks.protection.outlook.com/?url=http%3A%2F%2Fwww.ncbi.nlm.nih.gov%2Fbioproject%2F1128363&data=05%7C02%7Cmaria.bergsland%40ki.se%7C19695f33be0d4f103eec08dc95a735ba%7Cbff7eef1cf4b4f32be3da1dda043c05d%7C0%7C0%7C638549792599433064%7CUnknown%7CTWFpbGZsb3d8eyJWIjoiMC4wLjAwMDAiLCJQIjoiV2luMzIiLCJBTiI6Ik1haWwiLCJXVCI6Mn0%3D%7C0%7C%7C%7C&sdata=qUtIvc38c2exq3YN5gI0YSf%2BaDbm7Hy3H%2FR0iDoeKpU%3D&reserved=0

Acknowledgement

J.M is supported by grants from the Swedish Research Council, The Swedish Cancer Foundation, The Swedish Child Cancer Foundation, The Swedish Brain Foundation. E.R was supported by a Postdoctoral fellowship supported by the Wenner-Gren Foundation The research was supported by the National Genomics Infrastructure in Stockholm (funded by Science for Life Laboratory, the Knut and Alice Wallenberg Foundation, and the Swedish Research Council) and NAISS/Uppsala Multidisciplinary Center for Advanced Computational Science for assistance with massively parallel sequencing and access to the UPPMAX computational infrastructure.

References

1. Ostrom, Q. T. *et al.* CBTRUS Statistical Report: Primary Brain and Other Central Nervous System Tumors Diagnosed in the United States in 2015–2019. *Neuro-Oncol.* **24**, v1–v95 (2022).

2. Chen, J. *et al.* A restricted cell population propagates glioblastoma growth after chemotherapy. *Nature* **488**, 522–526 (2012).

3. Lan, X. *et al.* Fate mapping of human glioblastoma reveals an invariant stem cell hierarchy. *Nature* **549**, 227–232 (2017).

4. Singh, S. K. *et al.* Identification of human brain tumour initiating cells. *Nature* **432**, 396–401 (2004).

5. Rocha, A. M. A. de la, Sampron, N., Alonso, M. M. & Matheu, A. Role of SOX family of transcription factors in central nervous system tumors. *Am. J. cancer Res.* **4**, 312–24 (2014).

6. Yang, R. *et al.* POU2F2 regulates glycolytic reprogramming and glioblastoma progression via PDPK1-dependent activation of PI3K/AKT/mTOR pathway. *Cell Death Dis.* **12**, 433 (2021).

7. Giannopoulou, A.-I., Kanakoglou, D. S. & Piperi, C. Transcription Factors with Targeting Potential in Gliomas. *Int. J. Mol. Sci.* **23**, 3720 (2022).

8. Wang, L. *et al.* A single-cell atlas of glioblastoma evolution under therapy reveals cell-intrinsic and cell-extrinsic therapeutic targets. *Nat. Cancer* **3**, 1534–1552 (2022).

9. Marques, C. *et al.* NF1 regulates mesenchymal glioblastoma plasticity and aggressiveness through the AP-1 transcription factor FOSL1. *eLife* **10**, e64846 (2021).

10. Richards, L. M. *et al.* Gradient of Developmental and Injury Response transcriptional states defines functional vulnerabilities underpinning glioblastoma heterogeneity. *Nat. Cancer* **2**, 157–173 (2021).

11. Hagey, D. W., Bergsland, M. & Muhr, J. SOX2 transcription factor binding and function. *Development* **149**, (2022).

12. Sarkar, A. & Hochedlinger, K. The Sox Family of Transcription Factors: Versatile Regulators of Stem and Progenitor Cell Fate. *Cell Stem Cell* **12**, 15–30 (2013).

13. Shaulian, E. & Karin, M. AP-1 as a regulator of cell life and death. *Nat. Cell Biol.* **4**, E131–E136 (2002).

14. Sandberg, M., Källström, M. & Muhr, J. Sox21 promotes the progression of vertebrate neurogenesis. *Nat Neurosci* **8**, 995–1001 (2005).

15. Kurtsdotter, I. *et al.* SOX5/6/21 Prevent Oncogene-Driven Transformation of Brain Stem Cells. *Cancer Res* **77**, 4985–4997 (2017).

16. Caglayan, D., Lundin, E., Kastemar, M., Westermark, B. & Ferletta, M. Sox21 inhibits glioma progression in vivo by forming complexes with Sox2 and stimulating aberrant differentiation. *Int J Cancer* **133**, 1345–1356 (2013).

17. Wang, Q. *et al.* Tumor Evolution of Glioma-Intrinsic Gene Expression Subtypes Associates with Immunological Changes in the Microenvironment. *Cancer Cell* **32**, 42-56.e6 (2017).

18. Verhaak, R. G. W. *et al.* Integrated Genomic Analysis Identifies Clinically Relevant Subtypes of Glioblastoma Characterized by Abnormalities in PDGFRA, IDH1, EGFR, and NF1. *Cancer Cell* **17**, 98–110 (2010).

19. Redelsperger, I. M. *et al.* Stability of Doxycycline in Feed and Water and Minimal Effective Doses in Tetracycline-Inducible Systems. *J. Am. Assoc. Lab. Anim. Sci. : JAALAS* **55**, 467–74 (2016).

20. Olmez, I. *et al.* Combined c-Met/Trk inhibition overcomes resistance to CDK4/6 inhibitors in Glioblastoma. *Cancer Res.* **78**, canres.3124.2017 (2018).

21. Krusche, B. *et al.* EphrinB2 drives perivascular invasion and proliferation of glioblastoma stem-like cells. *eLife* **5**, e14845 (2016).

22. Yang, R. *et al.* HDAC9 promotes glioblastoma growth via TAZ-mediated EGFR pathway activation. *Oncotarget* **6**, 7644–7656 (2015).

23. Gangemi, R. M. R. *et al.* SOX2 Silencing in Glioblastoma Tumor-Initiating Cells Causes Stop of Proliferation and Loss of Tumorigenicity. *Stem Cells* **27**, 40–48 (2009).

24. Favaro, R. *et al.* Sox2 Is Required to Maintain Cancer Stem Cells in a Mouse Model of High-Grade Oligodendroglioma. *Cancer Res* **74**, 1833–1844 (2014).

25. Hagey, D. W. *et al.* CYCLIN-B1/2 and -D1 act in opposition to coordinate cortical progenitor self-renewal and lineage commitment. *Nat Commun* **11**, 2898 (2020).

26. Buenrostro, J. D., Giresi, P. G., Zaba, L. C., Chang, H. Y. & Greenleaf, W. J. Transposition of native chromatin for fast and sensitive epigenomic profiling of open chromatin, DNA-binding proteins and nucleosome position. *Nat. Methods* **10**, 1213–1218 (2013).

27. Soares, L. M. *et al.* Determinants of Histone H3K4 Methylation Patterns. *Mol. Cell* **68**, 773-785.e6 (2017).

28. Creyghton, M. P. *et al.* Histone H3K27ac separates active from poised enhancers and predicts developmental state. *Proc. Natl. Acad. Sci.* **107**, 21931–21936 (2010).

29. Makino, H. *et al.* A selective inhibition of c-Fos/activator protein-1 as a potential therapeutic target for intervertebral disc degeneration and associated pain. *Sci. Rep.* **7**, 16983 (2017).

30. Fanjul, A. *et al.* A new class of retinoids with selective inhibition of AP-1 inhibits proliferation. *Nature* **372**, 107–111 (1994).

31. Huang, C. *et al.* Blocking activator protein-1 activity, but not activating retinoic acid response element, is required for the antitumor promotion effect of retinoic acid. *Proc. Natl. Acad. Sci.* **94**, 5826–5830 (1997).

32. Stupp, R. *et al.* Radiotherapy plus Concomitant and Adjuvant Temozolomide for Glioblastoma. *New Engl J Medicine* **352**, 987–996 (2005).

33. Tang, F. *et al.* Chromatin profiles classify castration-resistant prostate cancers suggesting therapeutic targets. *Science* **376**, eabe1505 (2022).

34. Murthy, P. K. L. *et al.* Epigenetic basis of oncogenic-Kras-mediated epithelial-cellular proliferation and plasticity. *Dev. Cell* **57**, 310-328.e9 (2022).

35. Carro, M. S. *et al.* The transcriptional network for mesenchymal transformation of brain tumours. *Nature* **463**, 318–325 (2010).

36. Bejjani, F., Evanno, E., Zibara, K., Piechaczyk, M. & Jariel-Encontre, I. The AP-1 transcriptional complex: Local switch or remote command? *Biochim. Biophys. Acta (BBA) - Rev. Cancer* **1872**, 11–23 (2019).

37. Ito, T. *et al.* Identification of SWI·SNF Complex Subunit BAF60a as a Determinant of the Transactivation Potential of Fos/Jun Dimers*. *J. Biol. Chem.* **276**, 2852–2857 (2001).

38. Bass, A. J. *et al.* SOX2 is an amplified lineage-survival oncogene in lung and esophageal squamous cell carcinomas. *Nat Genet* **41**, 1238–1242 (2009).

39. Rudin, C. M. *et al.* Comprehensive genomic analysis identifies SOX2 as a frequently amplified gene in small-cell lung cancer. *Nat Genet* **44**, 1111–1116 (2012).

40. Boumahdi, S. *et al.* SOX2 controls tumour initiation and cancer stem-cell functions in squamous-cell carcinoma. *Nature* **511**, 246–250 (2014).

41. Kareta, M. S. *et al.* Inhibition of Pluripotency Networks by the Rb Tumor Suppressor Restricts Reprogramming and Tumorigenesis. *Cell Stem Cell* **16**, 39–50 (2015).

42. Liu, Y. *et al.* A predominant enhancer co-amplified with the SOX2 oncogene is necessary and sufficient for its expression in squamous cancer. *Nat. Commun.* **12**, 7139 (2021).

43. Sathyan, P. *et al.* Mir-21–Sox2 Axis Delineates Glioblastoma Subtypes with Prognostic Impact. *J. Neurosci.* **35**, 15097–15112 (2015).

44. Uchikawa, M., Kamachi, Y. & Kondoh, H. Two distinct subgroups of Group B Sox genes for transcriptional activators and repressors: their expression during embryonic organogenesis of the chicken. *Mech. Dev.* **84**, 103–120 (1999).

45. Benedetti, V. *et al.* A SOX2-engineered epigenetic silencer factor represses the glioblastoma genetic program and restrains tumor development. *Sci. Adv.* **8**, eabn3986 (2022).

46. Kondoh, H. & Kamachi, Y. SOX–partner code for cell specification: Regulatory target selection and underlying molecular mechanisms. *Int J Biochem Cell Biology* **42**, 391–399 (2010).

47. Nishimoto, M., Fukushima, A., Okuda, A. & Muramatsu, M. The Gene for the Embryonic Stem Cell Coactivator UTF1 Carries a Regulatory Element Which Selectively Interacts with a Complex Composed of Oct-3/4 and Sox-2. *Mol Cell Biol* **19**, 5453–5465 (1999).

48. Boyer, L. A. *et al.* Core Transcriptional Regulatory Circuitry in Human Embryonic Stem Cells. *Cell* **122**, 947–956 (2005).

49. Tanaka, S. *et al.* Interplay of SOX and POU Factors in Regulation of the Nestin Gene in Neural Primordial Cells. *Mol. Cell. Biol.* **24**, 8834–8846 (2004).

50. Wu, J. *et al.* Transcardiac Perfusion of the Mouse for Brain Tissue Dissection and Fixation. *BIO-Protoc.* **11**, e3988 (2021).

51. Network, C. G. A. R. *et al.* Comprehensive, Integrative Genomic Analysis of Diffuse Lower-Grade Gliomas. *N. Engl. J. Med.* **372**, 2481–2498 (2015).

52. Team, R. C. R: A Language and Environment for Statistical Computing_. R Foundation for Statistical Computing. Preprint at https://www.R-project.org/ (2023).

53. Bergsland, M. *et al.* Sequentially acting Sox transcription factors in neural lineage development. *Gene Dev* **25**, 2453–2464 (2011).

54. Bailey, T. L. & Machanick, P. Inferring direct DNA binding from ChIP-seq. *Nucleic Acids Res.* **40**, e128–e128 (2012).

55. Zhao, H. *et al.* CrossMap: a versatile tool for coordinate conversion between genome assemblies. *Bioinformatics* **30**, 1006–1007 (2014).

56. Ye, T. *et al.* seqMINER: an integrated ChIP-seq data interpretation platform. *Nucleic Acids Res.* **39**, e35–e35 (2011).

57. McLean, C. Y. *et al.* GREAT improves functional interpretation of cis-regulatory regions. *Nat. Biotechnol.* **28**, 495–501 (2010).

58. Heinz, S. *et al.* Simple Combinations of Lineage-Determining Transcription Factors Prime cis-Regulatory Elements Required for Macrophage and B Cell Identities. *Mol. Cell* **38**, 576–589 (2010).

59. Stark, R., Brown & G. DiffBind: differential binding analysis of ChIP-Seq peak data. Preprint at http://bioconductor.org/packages/release/bioc/vignettes/DiffBind/inst/doc/DiffBind.pdf. (2011).

60. Bentsen, M. *et al.* ATAC-seq footprinting unravels kinetics of transcription factor binding during zygotic genome activation. *Nat. Commun.* **11**, 4267 (2020).

61. Love, M. I., Huber, W. & Anders, S. Moderated estimation of fold change and dispersion for RNA-seq data with DESeq2. *Genome Biol.* **15**, 550 (2014).

62. Blighe *et al.* EnhancedVolcano: publication-ready volcano plots with enhanced colouring and labeling. Preprint at https://github.com/kevinblighe/EnhancedVolcano. (2021).

63. Chen, J., Bardes, E. E., Aronow, B. J. & Jegga, A. G. ToppGene Suite for gene list enrichment analysis and candidate gene prioritization. *Nucleic Acids Res.* **37**, W305–W311 (2009).

Fig. 1

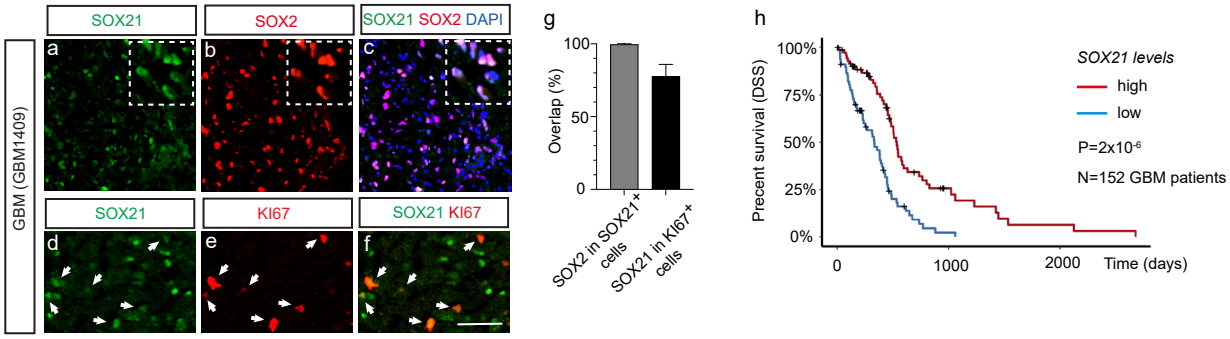
SOX21
SOX2
SOX21 SOX2 DAPI
GBM (GBM1409)
a
b
c
SOX21
KI67
SOX21 KI67
d
e
f
g
100
50
0
Overlap (%)
SOX2 in SOX21+ cells
SOX21 in KI67+ cells
h
100%
75%
50%
25%
0%
Precent survival (DSS)
0
1000
2000
Time (days)
SOX21 levels
high
low
P=2x10-6
N=152 GBM patients

Fig. 2

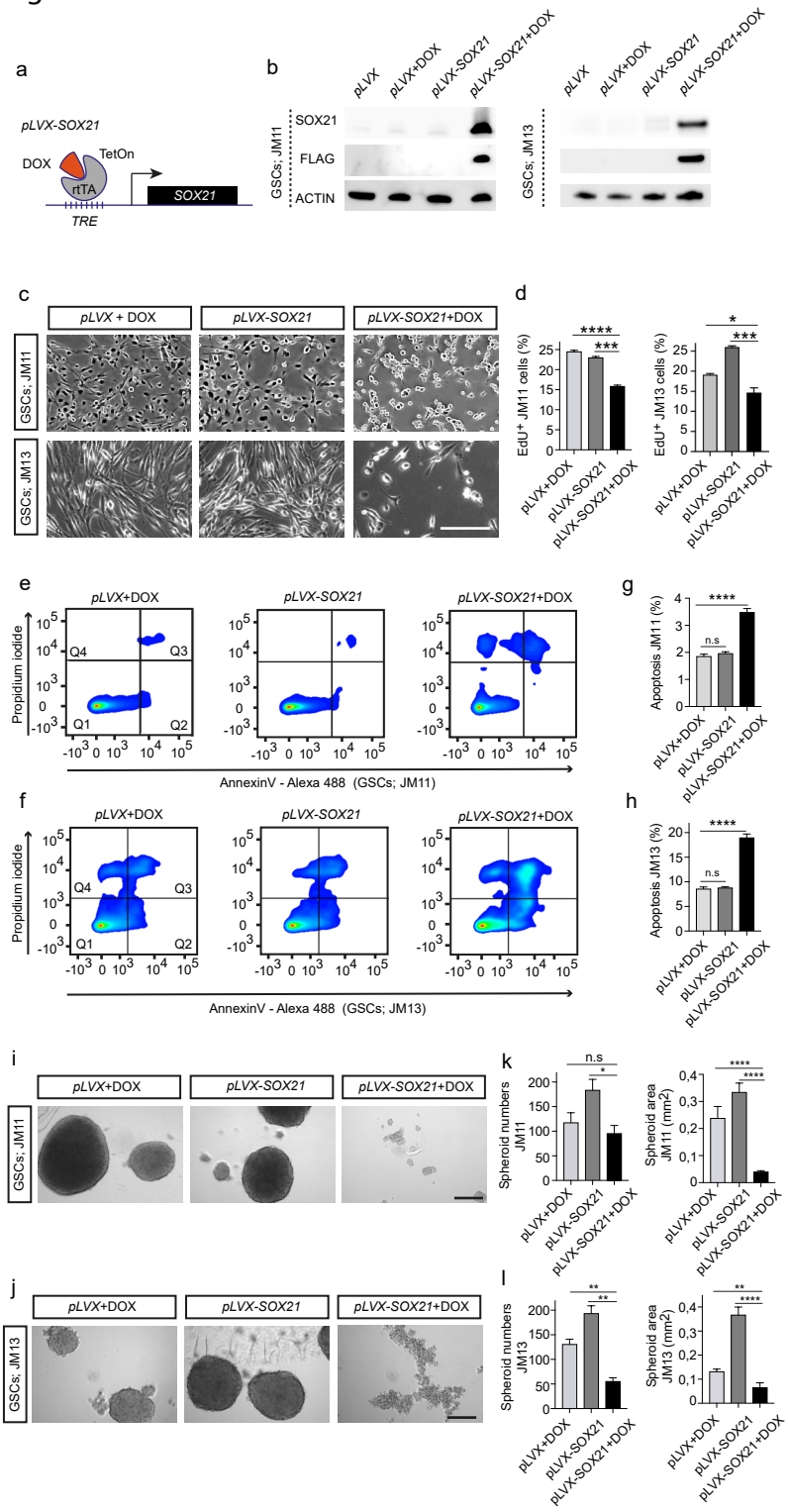
a
pLVX-SOX21
DOX
TetOn
rtTA
SOX21
TRE
b
pLVX
pLVX+DOX
pLVX-SOX21
pLVX-SOX21+DOX
GSCs; JM11
SOX21
FLAG
ACTIN
GSCs; JM13
c
pLVX + DOX
pLVX-SOX21
pLVX-SOX21+DOX
GSCs; JM11
GSCs; JM13
d
EdU+ JM11 cells (%)
EdU+ JM13 cells (%)
pLVX+DOX
pLVX-SOX21
pLVX-SOX21+DOX
e
pLVX+DOX
pLVX-SOX21
pLVX-SOX21+DOX
Propidium iodide
Q1
Q2
Q3
Q4
AnnexinV - Alexa 488 (GSCs; JM11)
g
Apoptosis JM11 (%)
n.s
f
AnnexinV - Alexa 488 (GSCs; JM13)
h
Apoptosis JM13 (%)
i
GSCs; JM11
k
Spheroid numbers JM11
Spheroid area JM11 (mm2)
j
GSCs; JM13
l
Spheroid numbers JM13
Spheroid area JM13 (mm2)

Fig. 3

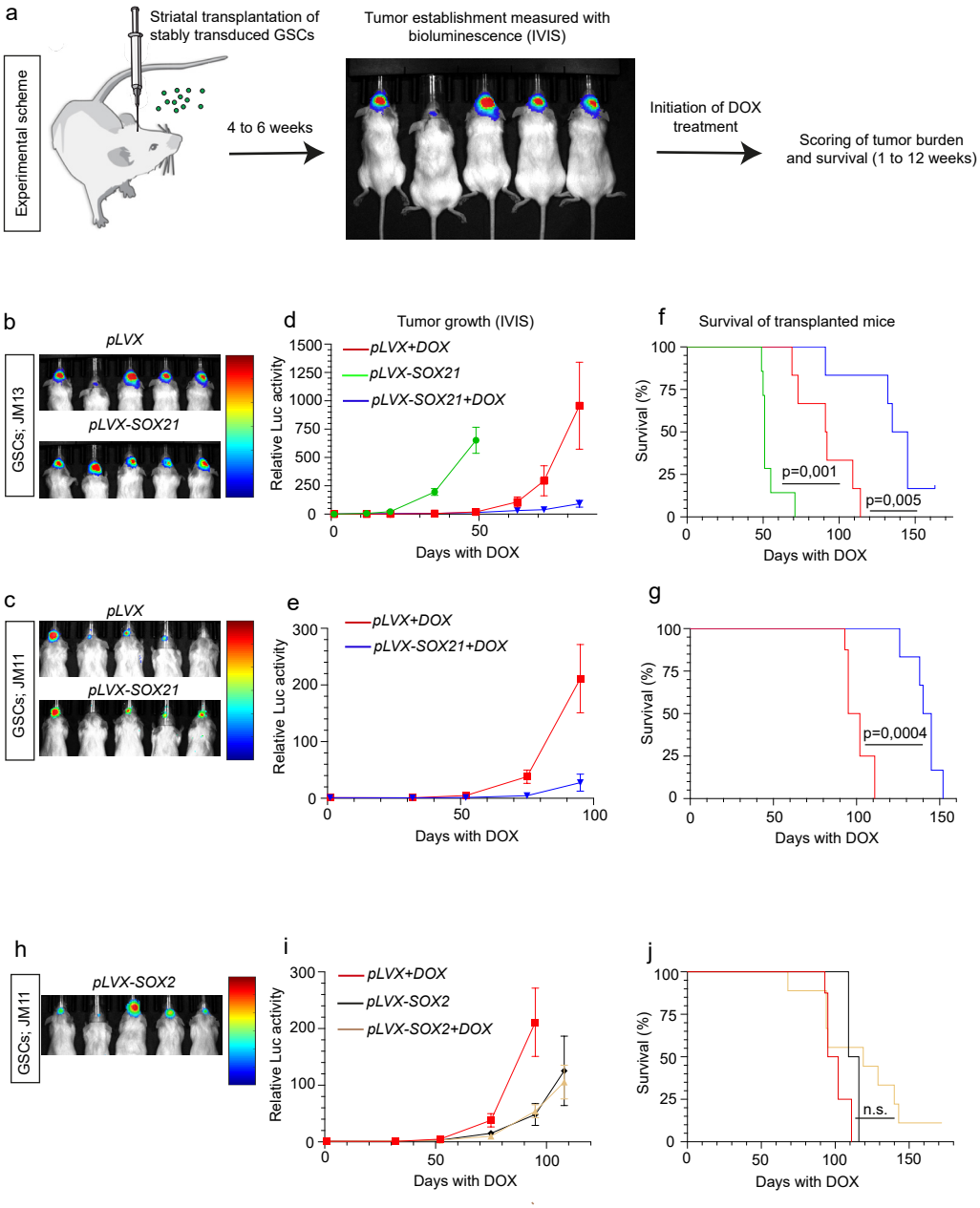
a
Experimental scheme
Striatal transplantation of stably transduced GSCs
4 to 6 weeks
Tumor establishment measured with bioluminescence (IVIS)
Initiation of DOX treatment
Scoring of tumor burden and survival (1 to 12 weeks)
b
GSCs; JM13
pLVX
pLVX-SOX21
c
GSCs; JM11
pLVX
pLVX-SOX21
d
Tumor growth (IVIS)
pLVX+DOX
pLVX-SOX21
pLVX-SOX21+DOX
Relative Luc activity
Days with DOX
e
pLVX+DOX
pLVX-SOX21+DOX
Relative Luc activity
Days with DOX
f
Survival of transplanted mice
Survival (%)
p=0,001
p=0,005
Days with DOX
g
Survival (%)
p=0,0004
Days with DOX
h
GSCs; JM11
pLVX-SOX2
i
pLVX+DOX
pLVX-SOX2
pLVX-SOX2+DOX
Relative Luc activity
Days with DOX
j
Survival (%)
n.s.
Days with DOX

Fig. 4

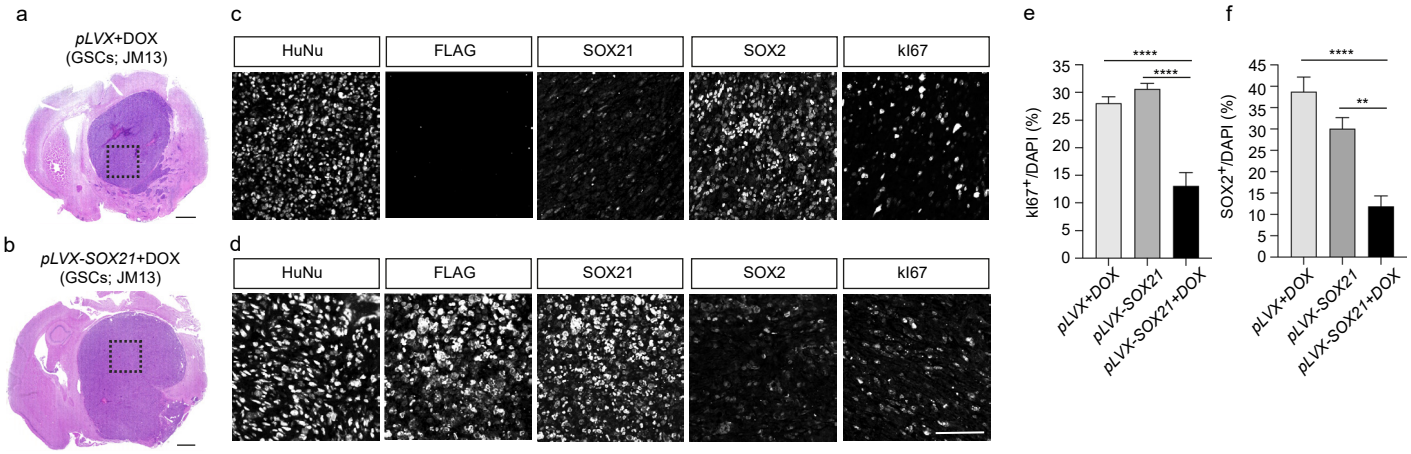
a
pLVX+DOX
(GSCs; JM13)
b
pLVX-SOX21+DOX
(GSCs; JM13)
c
HuNu
FLAG
SOX21
SOX2
kI67
d
HuNu
FLAG
SOX21
SOX2
kI67
e
kI67+/DAPI (%)
35
30
25
20
15
10
5
0
****
****
pLVX+DOX
pLVX-SOX21
pLVX-SOX21+DOX
f
SOX2+/DAPI (%)
45
40
35
30
25
20
15
10
5
0
****
**
pLVX+DOX
pLVX-SOX21
pLVX-SOX21+DOX

Fig. 5

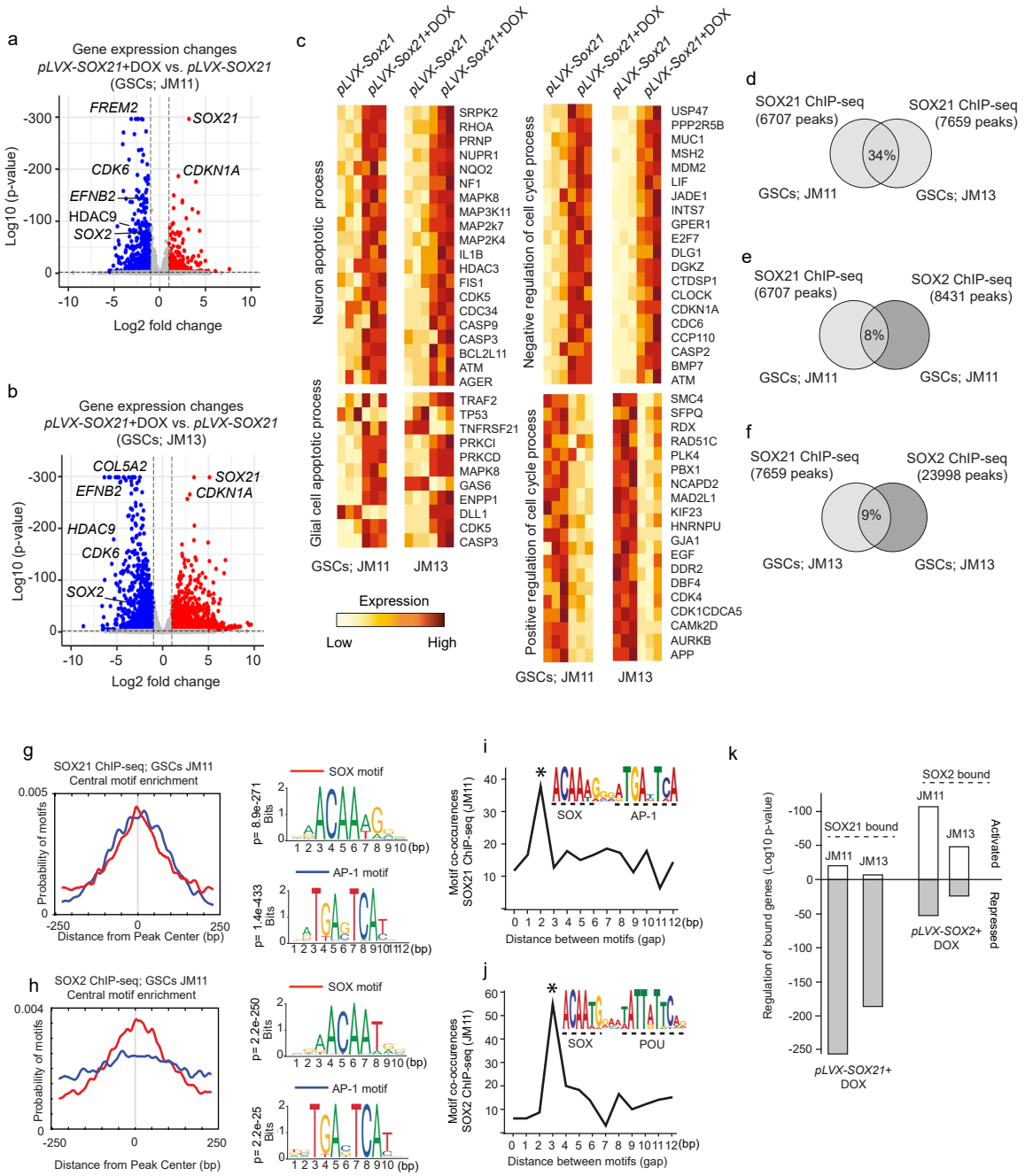
a
Gene expression changes
pLVX-SOX21+DOX vs. pLVX-SOX21
(GSCs; JM11)
FREM2
SOX21
CDK6
CDKN1A
EFNB2
HDAC9
SOX2
Log10 (p-value)
Log2 fold change
b
Gene expression changes
pLVX-SOX21+DOX vs. pLVX-SOX21
(GSCs; JM13)
COL5A2
SOX21
EFNB2
CDKN1A
HDAC9
CDK6
SOX2
Log10 (p-value)
Log2 fold change
c
pLVX-Sox21
pLVX-Sox21+DOX
Neuron apoptotic process
Glial cell apoptotic process
Negative regulation of cell cycle process
Positive regulation of cell cycle process
SRPK2
RHOA
PRNP
NUPR1
NQO2
NF1
MAPK8
MAP3K11
MAP2k7
MAP2K4
IL1B
HDAC3
FIS1
CDK5
CDC34
CASP9
CASP3
BCL2L11
ATM
AGER
TRAF2
TP53
TNFRSF21
PRKCI
PRKCD
MAPK8
GAS6
ENPP1
DLL1
CDK5
CASP3
USP47
PPP2R5B
MUC1
MSH2
MDM2
LIF
JADE1
INTS7
GPER1
E2F7
DLG1
DGKZ
CTDSP1
CLOCK
CDKN1A
CDC6
CCP110
CASP2
BMP7
ATM
SMC4
SFPQ
RDX
RAD51C
PLK4
PBX1
NCAPD2
MAD2L1
KIF23
HNRNPU
GJA1
EGF
DDR2
DBF4
CDK4
CDK1CDCA5
CAMk2D
AURKB
APP
GSCs; JM11
JM13
Expression
Low
High
d
SOX21 ChIP-seq
(6707 peaks)
SOX21 ChIP-seq
(7659 peaks)
34%
GSCs; JM11
GSCs; JM13
e
SOX21 ChIP-seq
(6707 peaks)
SOX2 ChIP-seq
(8431 peaks)
8%
GSCs; JM11
GSCs; JM11
f
SOX21 ChIP-seq
(7659 peaks)
SOX2 ChIP-seq
(23998 peaks)
9%
GSCs; JM13
GSCs; JM13
g
SOX21 ChIP-seq; GSCs JM11
Central motif enrichment
Probability of motifs
Distance from Peak Center (bp)
SOX motif
p= 8.9e-271
AP-1 motif
p= 1.4e-433
h
SOX2 ChIP-seq; GSCs JM11
Central motif enrichment
Probability of motifs
Distance from Peak Center (bp)
SOX motif
p= 2.2e-250
AP-1 motif
p= 2.2e-25
i
Motif co-occurences
SOX21 ChIP-seq (JM11)
SOX
AP-1
Distance between motifs (gap)
j
Motif co-occurences
SOX2 ChIP-seq (JM11)
SOX
POU
Distance between motifs (gap)
k
SOX2 bound
SOX21 bound
JM11
JM13
Activated
Repressed
Regulation of bound genes (Log10 p-value)
pLVX-SOX2+
DOX
pLVX-SOX21+
DOX

Fig. 6

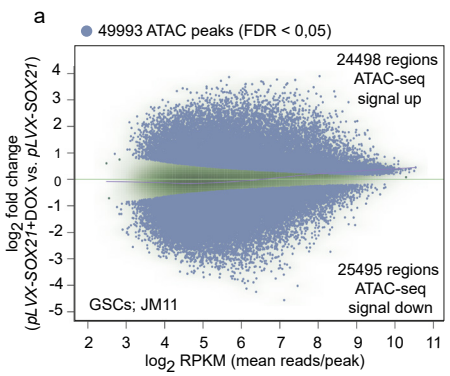

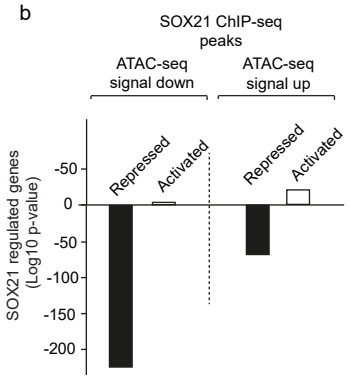

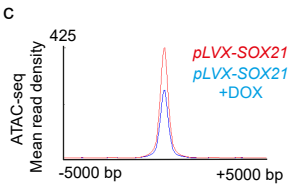

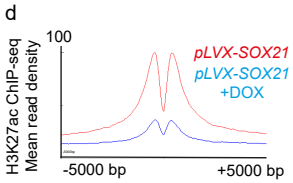

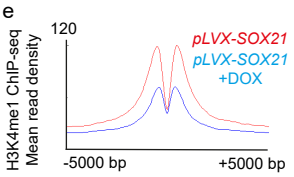

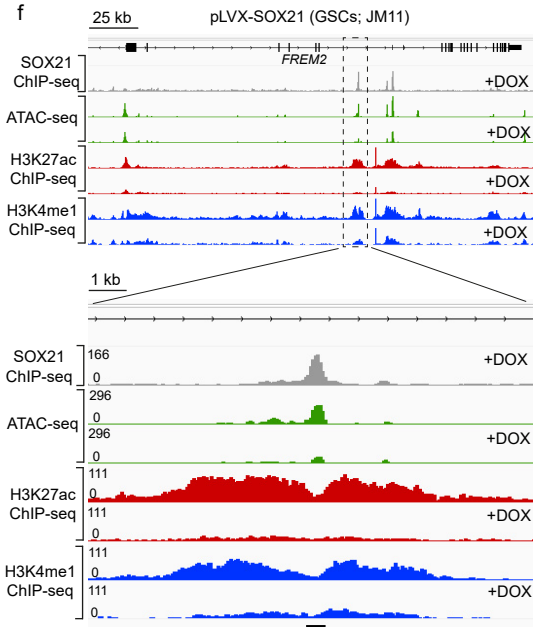

g

Motif enrichment in condensed chromatin
(SOX21 targeted vs. non-targeted chromatin)

Motifs	Transcription factor	P-value	% of targets
	AP-1	1e-575	47%
	SOX	1e-294	72%
	SOX	1e-61	22%

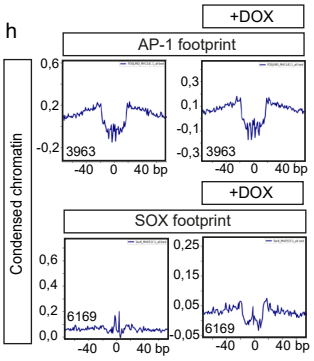

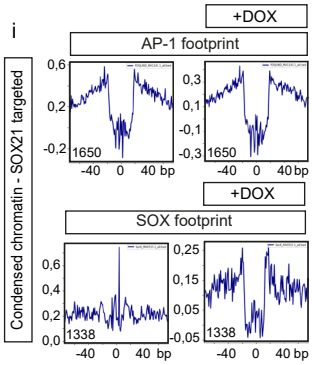

Fig. 7

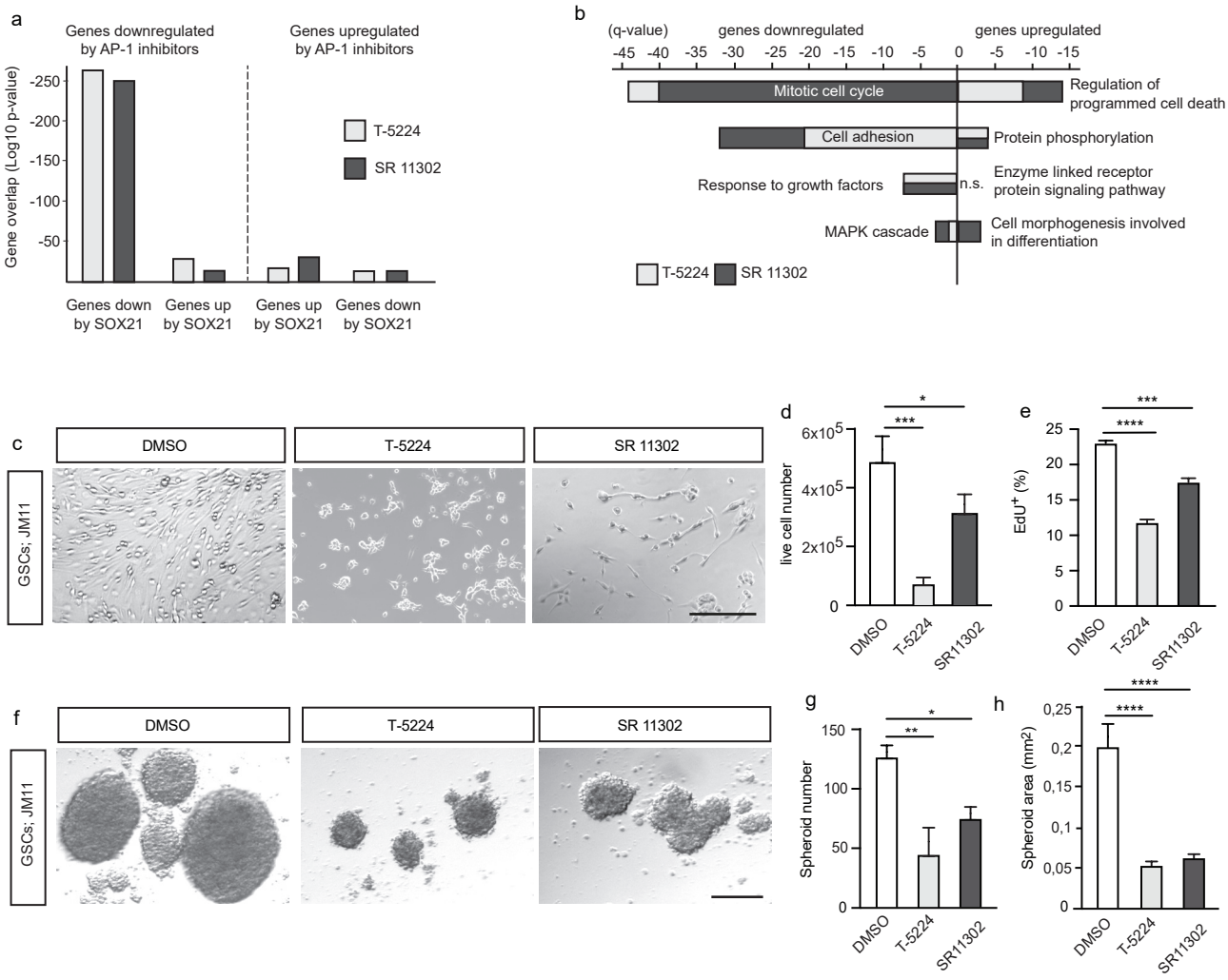
a
Genes downregulated by AP-1 inhibitors
Genes upregulated by AP-1 inhibitors
Gene overlap (Log10 p-value)
-250
-200
-150
-100
-50
T-5224
SR 11302
Genes down by SOX21
Genes up by SOX21
Genes up by SOX21
Genes down by SOX21
b
(q-value)
genes downregulated
genes upregulated
-45 -40 -35 -30 -25 -20 -15 -10 -5 0 -5 -10 -15
Mitotic cell cycle
Regulation of programmed cell death
Cell adhesion
Protein phosphorylation
Response to growth factors
n.s.
Enzyme linked receptor protein signaling pathway
MAPK cascade
Cell morphogenesis involved in differentiation
T-5224
SR 11302
c
DMSO
T-5224
SR 11302
GSCs; JM11
d
live cell number
6x10^5
4x10^5
2x10^5
0
*
***
DMSO
T-5224
SR11302
e
EdU+ (%)
25
20
15
10
5
0
***
****
DMSO
T-5224
SR11302
f
DMSO
T-5224
SR 11302
GSCs; JM11
g
Spheroid number
150
100
50
0
*
**
DMSO
T-5224
SR11302
h
Spheroid area (mm²)
0,25
0,2
0,15
0,1
0,05
0
****
****
DMSO
T-5224
SR11302